JOURNAL OF MATERIALS SCIENCE 15 (1980) 449–462

High-temperature fracture and diffusional deformation mechanisms in Si-Al-O-N ceramics

B. S. B. KARUNARATNE, M. H. LEWIS
Department of Physics, University of Warwick, Coventry, UK

A comparison has been made of hot-pressed Si–Al–O–N ceramics, with different impurity sintering aids (MgO and Mn_3O_4), in relation to microstructure, high-temperature creep and fracture. The Mn-containing ceramic exhibits a mechanism for creep of grain-boundary sliding accompanied by cavitation at triple junctions, nucleated within an impurity silicate residue. The measured non-integral stress exponent ($n \sim 1.5$) and activation energy Q in the creep equation $\dot{\epsilon} = \text{const.}\ \sigma^n \exp(-Q/kT)$ are typical of commercial silicon nitrides. A similar cavity-interlinkage is the principal mechanism for sub-critical crack growth, characterized by a low value for the stress-intensity exponent (n) in the relation V (crack velocity) = const. K_1^n determined on double-torsion test specimens. Triple-junction silicate, and hence cavitation, is absent in the Mg-containing ceramic, which exhibits a Coble diffusional creep mechanism (stress exponent $n = 1$). Sub-critical crack growth occurs only over a narrow range of stress intensity, near to K_{1C} with $n \sim 13$ in the $V - K_1^n$ relation. A grain-boundary de-segregation caused mainly by extraction of impurities into an oxide film results in further improvement in creep and resistance to sub-critical crack growth.

1. Introduction

Polycrystalline ceramic materials based on the β-Si_3N_4 crystal structure have a unique combination of properties which has encouraged their potential application as engineering components under conditions of high stress and temperature. The crystal structure has a low thermal expansion coefficient, an intrinsic lack of crystal plasticity dictated by the highly covalent Si–N bond and an oxidation resistance conferred by a self-healing SiO_2 film. However, the high-temperature strength and oxidation resistance of the polycrystalline ceramic are dominated by the properties of the intercrystalline bond, which in turn is sensitive to the presence of "impurity" segregation, an unavoidable result of the fabrication mechanism. A key question is, therefore, to what extent can intercrystalline cohesion be improved to approach that conferred by the ideal Si–N bond, i.e. is there a limitation imposed by the distortion of bond length and directionality in the pure grain boundary which may show little improvement from the severely segregated state?

In this paper we will demonstrate that the cohesive and transport properties of β-Si_3N_4 grain boundaries are sensitive to concentration and chemical species of impurity segregant. In particular, we wish to point out that the properties of hot-pressed Al- and O-substituted forms of β-Si_3N_4 [1] are unique in the ability to control grain-boundary properties, resulting both in the control of high-temperature crack propagation and a clarification of mechanisms for deformation throughout the range of ceramics based on β-Si_3N_4.

One of the major problems concerning the high-temperature engineering application of ceramics is that of delayed fracture which is characterized by the slow growth of pre-existing flaws at stresses much lower than for fast (instantaneous) crack propagation. Attempts have been made [2–4] to quantify this effect via the relation between measured crack velocity (V) and a "fracture

0022–2461/80/020449–14$03.40/0

mechanics" parameter (K_I), which is a measure of the stress intensity at the tip of the slowly-moving crack. The relationship is empirical and no rigorous theory has yet explained the fit to an equation of the type; $V = A \cdot K_I^n \exp(-Q/kT)$ where $n \gg 1$ and is dependent on the rate controlling fracture mechanism. The empirical determination of this relationship for a ceramic has its major use in predicting the lifetime of an engineering component before catastrophic fracture [3]. However, in this research, it has been used to distinguish between different sub-critical crack growth mechanisms via the exponent n and hence to relate this behaviour to differences in creep deformation mechanism for ceramics with different grain-boundary-segregated impurity content.

2. Microstructures

The research is based on two hot-pressed Si–Al–O–N ceramics which have a carefully "balanced" O/N ratio to achieve the single phase condition corresponding to the substituted β' crystal composition $Si_{6-x}Al_xO_xN_{8-x}$ [1]. Both ceramics have a substitution level of $x \approx 1$ but differ in the composition of the additive used to enhance the densification process. 1 wt% MgO has been added to the first ceramic (specimen C) to assist in the formation of a Mg-silicate liquid-sintering medium, the components of which are progressively removed via solution in β' crystals. The microstructure, which has been described previously [1], is a single phase $\sim 1\,\mu m$ grain-size β' ceramic with no detectable grain-boundary residual phase (using high-resolution electron-microscopy). However, there is some segregation of Mg, O and impurity Ca detectable via Auger electron spectroscopy.

A second ceramic (specimens A and B prepared separately) contains a mixed MgO/Mn_3O_4 additive which further improves the ease of densification, probably via a reduction in the silicate liquidus and viscosity during the reactive-liquid sintering mechanism. The microstructure of this ceramic [5] contains a similar 1 μm β' grain size to specimen C, but some of the Mn appears in the form of a low density of grain-boundary silicide particles together with impurity Fe. This heterogeneity, although on a coarse scale (only a small fraction of grain boundaries contain particles), prevents a more precise determination of the general grain-boundary segregation layer by low spatial resolution Auger spectroscopy. However, Mg, O and impurity Ca appear in the Auger spectrum from high-temperature fracture surfaces, together with Mn. Recent high-resolution electron microscopy has detected extremely small (< 1000 Å) regions of triple-junction glass (a residue of the silicate liquid sintering aid) which is not present in specimen C (Fig. 1a and b). This is believed to be important in determining the markedly different creep and fracture behaviour of the two materials. Apart from the triple junctions, there is no resolvable difference between β' grain boundaries in the two ceramics, down to an approximate limit set by the prism-plane spacing (6.6 Å) in adjacent β' crystals (Fig. 1c and d). The "lattice" imaging technique

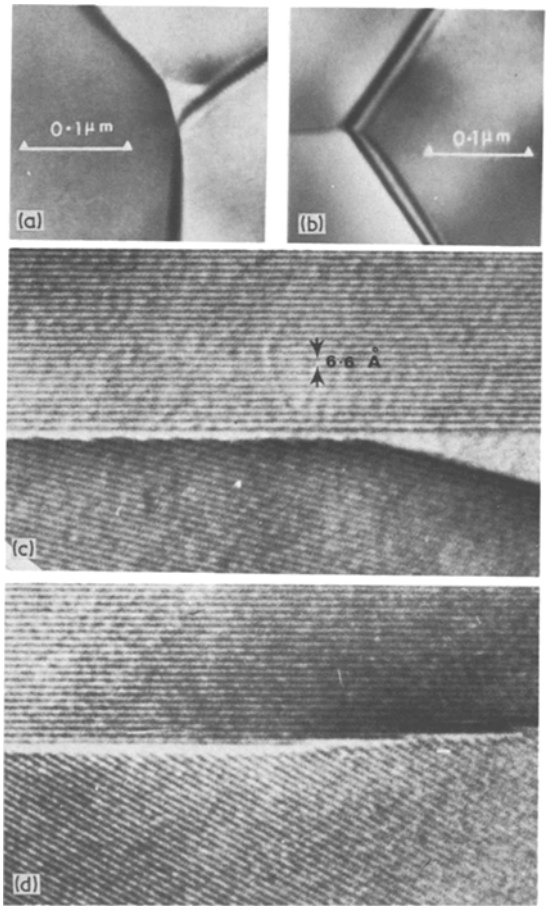

Figure 1 Transmission electron micrographs showing typical triple-junction structure, imaged in conventional diffraction contrast, for ceramics B and C (a and b respectively) and β'–β' interface structure "lattice"-imaged for ceramics B and C in (c) and (d), respectively. The lattice images are selected from a series of specimen tilt through small angles near the exact prism-plane diffraction condition to ensure parallelism between electron beam and grain boundary. In (d) the boundary is observed to deviate from the prism plane orientation.

has previously been used to study β–β grain boundaries in commercial Si_3N_4 ceramics, some of which contain silicate glass phase [6, 7]. The use of this technique may be criticised as being too selective in requiring pairs of non-parallel prism planes together with the boundary to be parallel to the incident electron beam. In many images [6] one of the grains has the prism plane parallel to the grain-boundary and this is believed to result from a preferred prism-plane faceted growth of β into the liquid silicate. It is significant that a high density of this special type of interface is observed in specimens A and B (e.g. Fig. 1c), whereas the boundary has a more random orientation in specimen C, making lattice-imaging much more difficult.

3. High-temperature creep

3.1. Macroscopic parameters

Fine grain-size ceramics composed of intrinsically strong crystals with covalent bonding, such as β-Si_3N_4 are expected to undergo diffusional creep identified by a stress exponent $n = 1$ in the generalized creep rate ($\dot{\epsilon}$) equation:

$$\dot{\epsilon} = \text{constant } \sigma^n \exp(-Q/kT),$$

where Q is the activation energy for diffusion through the crystal (Herring–Nabarro creep [8]) or via grain-boundaries (Coble creep [9]). For a ceramic material in which dislocation mobility is negligible, the creep mechanism may be viewed as that of grain-boundary sliding accommodated entirely by lattice or grain-boundary diffusion between "tensile" and "compressive" grain facets. Specific models for the sliding mechanism have been developed [10] which result in different values of the pre-exponential constant from that given by the Herring–Nabarro or Coble equations for large strains, but the stress exponents and activation energies are unchanged. Hence a problem is presented in interpreting high stress exponents ($n \sim 1.5$ to 2) in a number of ceramics, especially the range of commercially available β-Si_3N_4 ceramics (HS110, HS130, NC132 etc). The various mechanisms which have been suggested in explanation of the non-integral stress-exponent include a "non-Newtonian" grain-boundary sliding involving dislocation motion near the interface [11, 12] and void formation, associated with grain-boundary sliding via a silicate phase (in Si_3N_4), in modifying the internal stress [13, 14]. The absence of precise theory for comparison and a variability of the stress exponent do not permit unambiguous interpretation. The experimental work described here, in which the $n = 1$ stress exponent is achieved under specific conditions, enables a clarification of these ideas.

Fig. 2 shows a set of four-point bend–creep curves for various temperatures and stresses for Si–Al–O–N ceramics B and C with comparison plots for commercial Si_3N_4 and SiC ceramics. A derivation of creep mechanisms from data based on surface tensile stress and strain in four-point bend specimens (in which the stress system is inhomogeneous) may be subject to criticism. In this research the analyses of stress-exponents and activation energies have been repeated using uniaxial compression creep which has confirmed the earlier conclusions based on four-point analyses.

The creep curves demonstrate the marked differences in average creep rate $\dot{\epsilon}$, for a given temperature and stress, for the two ceramics (B and C) prepared with different additives, B being inferior to a high grade Si_3N_4 (HS130) and C approaching the extremely low creep rate of SiC [15] after a long "transient" period. Stress exponents (n) for Si–Al–O–N ceramic A and B, determined from incremental stress changes, exhibit non-integral ($n \sim 1.5$ to 1.6) values typical of commercial Si_3N_4 ceramics (Fig. 3a). These values are independent of sense of the changing stress (increasing or decreasing steps) when the experiments are conducted over conveniently short time intervals (typically changed with a periodicity of 24 h following a "primary" creep range of 20 to 40 h). This is contrary to the surprising observation for ceramic C of a change in stress exponent from $n < 1$ to $n > 1$, depending on the sense of the incremental stress change (Fig. 3b). This is explicable as a non-steady-state creep behaviour and discussed below in terms of a change in grain-boundary microstructure with time. After long times the measured exponent has the integral ($n = 1$) value consistent with a diffusional creep mechanism.

Analyses of activation energy for creep via incremental temperature tests confirm the differences between the Mn and Mg containing ceramics. A and B both exhibit activation energies of ~ 496 kJ mol^{-1} (Fig. 4a), whereas the long-term transient effect in specimen C results in an activation-energy plot (Fig. 4b) which has an increasing negative slope with increasing temperature and time and is sensitive to test environment. After very long times,

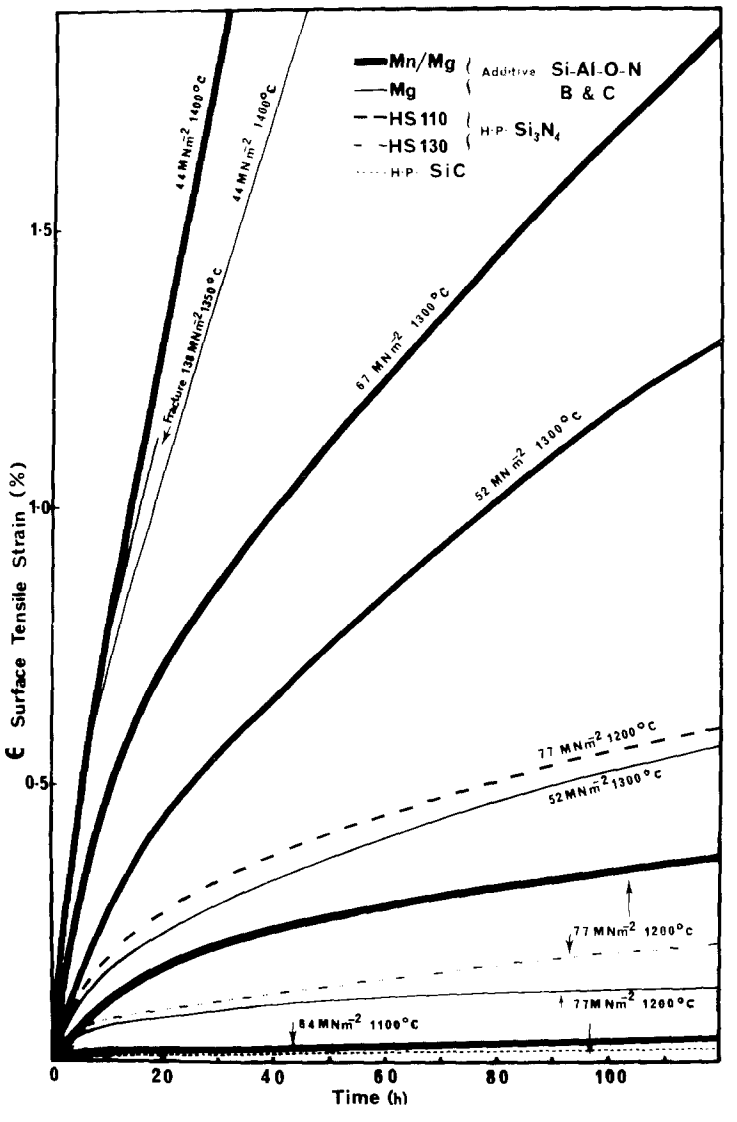

Figure 2 Four-point bend creep curves for Si–Al–O–N ceramics B and C at various temperatures and stresses compared with creep curves at ~ 1200° C for commercial Si_3N_4 ceramics and a hot-pressed SiC ceramic.

or in specimens pre-heat treated in an oxidizing environment, the gradient approaches a constant value ~ 830 kJ mol^{-1}, higher than previously measured for Si_3N_4 ceramics.

3.2. Creep mechanisms

Ceramics A and B which have non-integral ($n > 1$) stress exponents are observed to undergo extensive cavitation, initiated at grain triple-junctions throughout the range of creep strain. These are imaged in electron-transparent sections as isolated cavities (at low creep strains) which frequently have prism-plane facets formed via surface diffusion (Fig. 5a). At larger creep strains the cavities occupy whole grain facets, occasionally interconnecting to form large internal cracks. Thus the creep mechanism in these ceramics is likely to be that of grain-boundary sliding in which the shape-accommodation is partially via grain-boundary diffusion and partially via cavitation (Fig. 5b). Measurements of stress-exponent and activation energy under the condition of varying internal stress caused by cavitation is unlikely to provide a meaningful indication of rate-controlling mechanism. The observation of an approximately steady-state creep may be the result of the increasing effective stress (and hence creep rate) being compensated by an increased activation energy for diffusion along grain boundaries which, in turn, is caused by a progressive change in boundary impurity level and structure, similar to that proposed for ceramic C below.

Si–Al–O–N C is the first example of a β-Si_3N_4 type ceramic which exhibits a non-cavitating

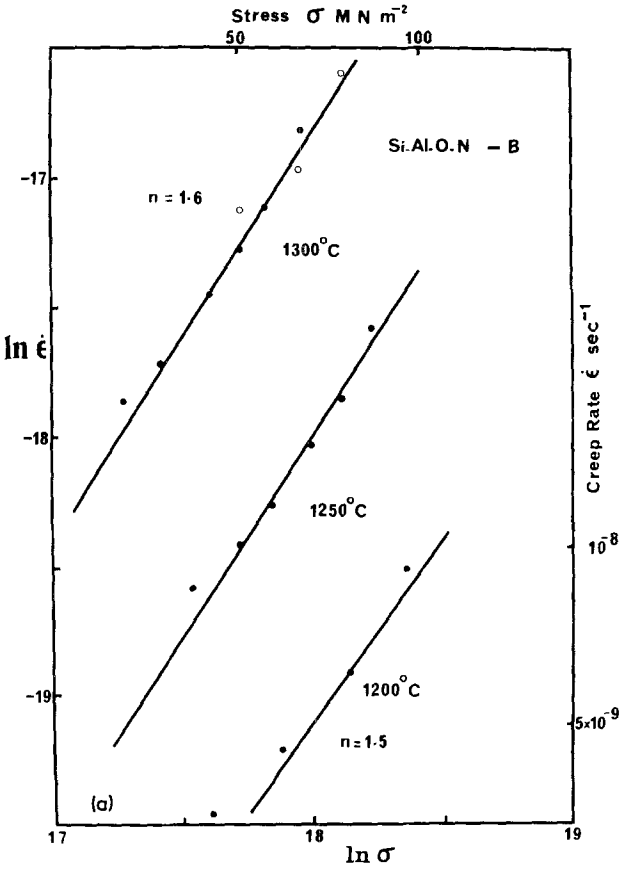

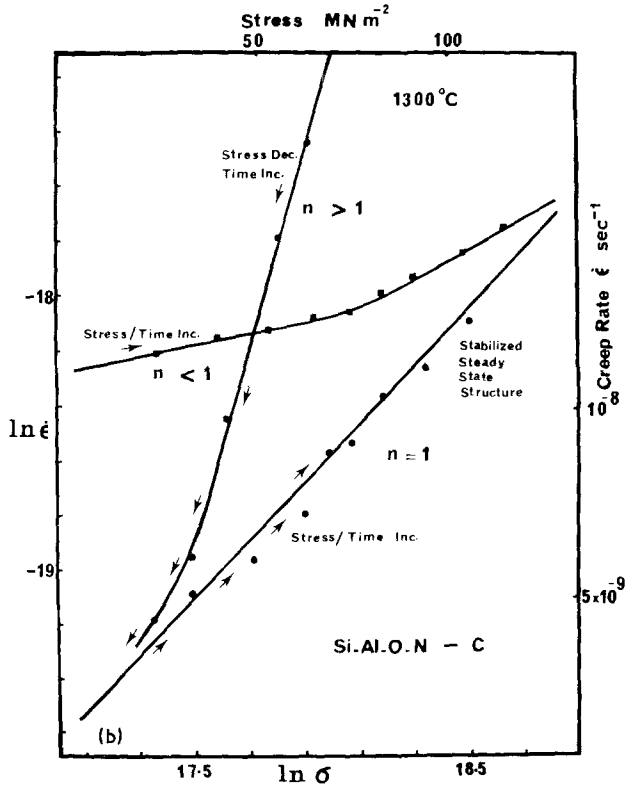

Figure 3 (a) Stress-exponents (n) for creep of ceramic B at various temperatures determined from incremental stress tests (open and closed circles at 1300° C are for two separate specimens. (b) Non-steady-state behaviour illustrated in determining values for n for ceramic C with increasing or decreasing stress increment (upper curves). The value of $n = 1$ characteristic of diffusional creep is obtained after long test times or for pre-heat treated specimens.

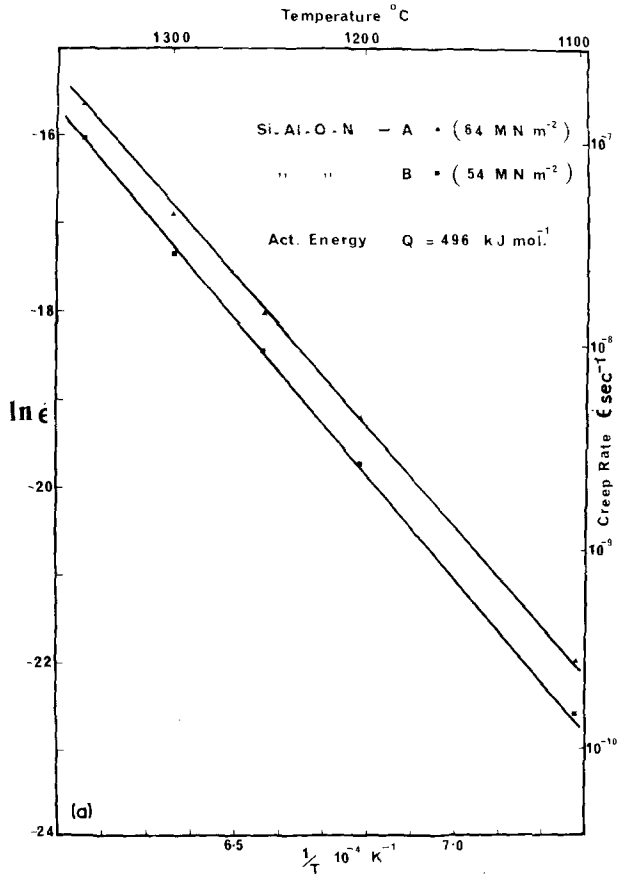

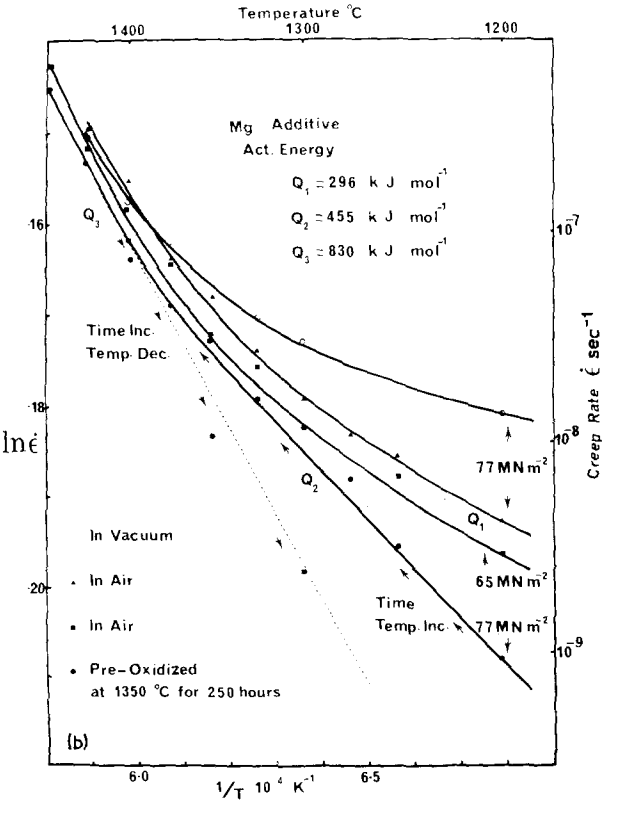

Figure 4 Determination of approximate activation energies for creep from incremental temperature tests. (a) Ceramics A and B; (b) ceramic C, showing the influence of the time-dependent change in grain-boundary structure, the influence of test environment and of a pre-heat treatment on the activation energy.

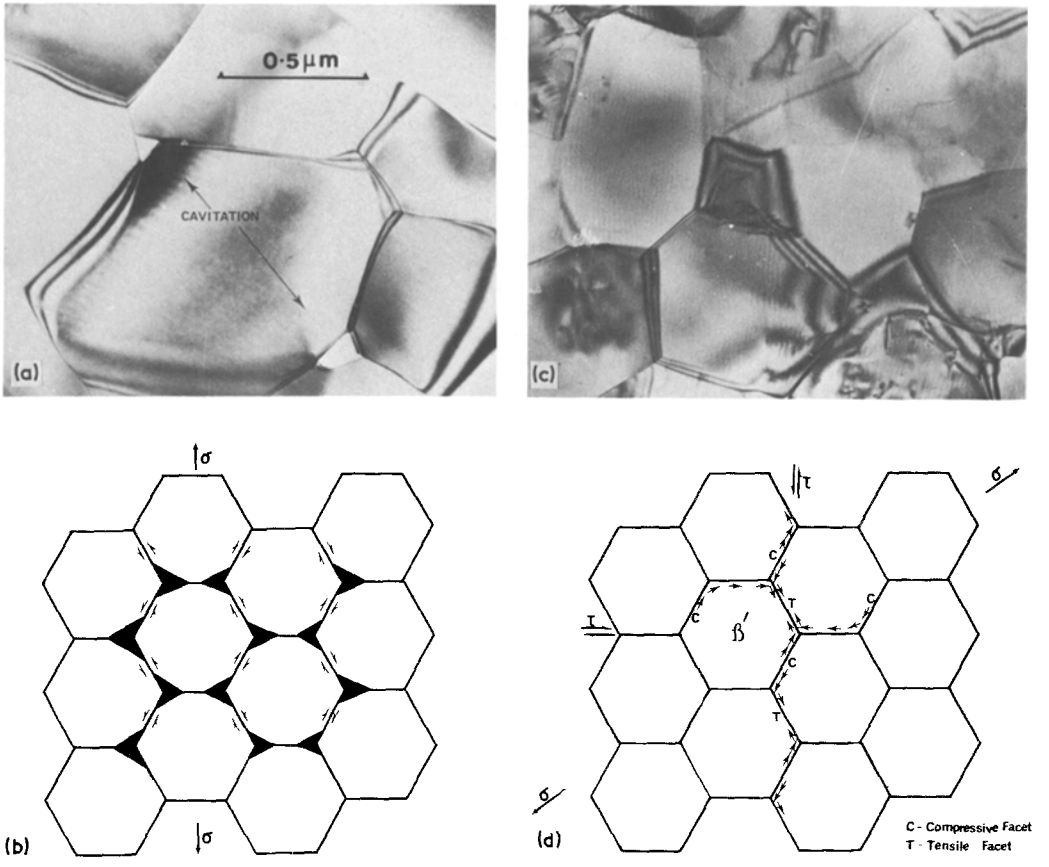

Figure 5 Transmission electron micrographs taken from creep test specimens of ceramics B and C (a and c respectively) with diagrams illustrating the diffusional accommodation of grain-boundary sliding (d) and the partial accommodation via cavitation (b) for ceramics C and B, respectively.

diffusional creep behaviour. Microstructures before and after creep deformation are indistinguishable (Fig. 5c). The evidence for a grain-boundary diffusional accommodation of sliding (Fig. 5d) is provided by the changing creep rate and measured activation energy, sensitivity to environment in the transient period, and a correlation with a rate-controlling mechanism for oxidation involving extraction of grain-boundary impurities into the SiO_2 surface layer [16, 17]. Hence the changing gradient with temperature in the activation-energy plot is not caused by a change in rate-controlling diffusion from grain-boundary to lattice (i.e. Coble to Herring–Nabarro creep), the activation energy for the latter being comparatively high in β' crystals which have predominantly covalent bonding. The sensitivity to environment also does not support the possibility of the changing creep rate resulting from grain growth (creep rate $\dot{\epsilon} \propto 1/d^3$ for the Coble mechanism such that mean grain size d would need to change by only $\sim 10\%$ to explain the observed extremes in $\dot{\epsilon}$ for a given temperature and stress). Further, there is no detectable change in mean grain-size for ceramics which have been heat-treated for > 1000 h at the test temperatures.

The major differences in creep behaviour between the two classes of ceramic A (or B) and C results from the presence or absence of intergranular creep cavitation. This is believed to be caused by the occurrence of microscopic (< 1000 Å) regions of triple-junction silicate glass phase which is a residue of the densification process. Cavities may nucleate within the triple junction phase at low stresses if the silicate is above its glass-transition temperature during the creep test. The Mg-containing ceramic (C) contains no detectable triple-junction glass and the cohesive energy of the grain-boundary is sufficient to prevent cavity nucleation up to the maximum stresses and temperatures studied. Grain-boundary cohesion is enhanced by a process of de-segregation of the grain-boundary impurities, thereby increasing

the density of covalent Si–N grain-boundary atomic bonds. The activation energies for grain-boundary diffusion of β' components (Si–Al–O–N) are simultaneously increased, resulting in the time-dependent reduction in creep rate and "artificial" values for n and Q. The "limiting" value of > 800 kJ mol^{-1} probably approaches that for diffusion of Si etc. (or some compound "molecular" species) within a "pure" β' grain boundary.

Although the grain-boundary de-segregation mechanism is discussed here in terms of outward impurity diffusion into a surface layer, an alternative mechanism of solid solution within β' crystals from an initially non-equilibrium distribution during fabrication, is believed to occur simultaneosly. However, in view of the time scale for the change in creep-rate, the dominant mechanism must involve oxidation, otherwise diffusion rates within β' crystals must be unrealistically slow (diffusion distances are less than the grain size of $\sim 1\,\mu$m). Typical solid-state diffusion rates would result in appreciable depletion of grain-boundary impurities within ~ 100 h to a depth of 1 to 2 mm, typical of bend and compression creep-test specimen widths.

4. High-temperature fracture

4.1. Sub-critical crack growth

The crack velocity (V)–stress intensity (K_1) relationships have been studied in the temperature interval, 1100 to 1400° C, in which extensive sub-critical crack growth has been observed during fracture toughness (K_{IC}) tests on the Mn-containing ceramic [5]. The construction of a double-torsion vacuum test jig and analytical procedures used in determining the K_1–V relationships are described in a separate paper [18]. In summary, data in the higher velocity region ($V \sim 10^{-2}$ to 10^{-4}) have been obtained via the rate of load–relaxation under fixed-grip conditions [19, 20], that for intermediate velocities using a constant displacement rate (cross-head velocity) on the Instron testing machine [2], and for low velocities (10^{-6} to 10^{-10}) by direct measurement of the crack-tip displacement on sequential loading [2]. In each case K_1 is calculated from the measured Instron load (P) and the specimen geometry (Fig. 6) from the relation [19],

$$K_1 = PW_m\left[\frac{3(1+\nu)}{Wd^3d_n}\right]^{1/2}$$

where $W_m = 5$ mm, $W = 15$ mm, $d = 2$ mm, and

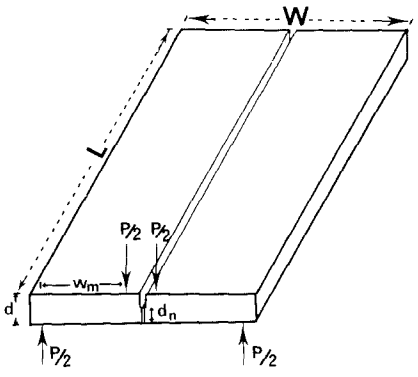

Figure 6 The "double-torsion" test specimen, characterized by the independence of stress intensity factor (K_1) on crack position, used in determining the crack velocity (V)–K_1 relationships at high temperatures.

$d_n = 1$ mm. Poissons ratio (ν) was calculated from the Young's and shear moduli (E and G) which were experimentally measured using a resonant bar method at 20° C.

The experimental K_1–V data are presented for both types of ceramic (B and C) in Fig. 7. There is an excellent fit to straight-line logarithmic plots for a given material and temperature and good continuity for a wide range of crack velocities using the different techniques. Ceramics B and C exhibit markedly different characteristics. The stress-intensity exponent for ceramic B has a single value ($n \sim 7$) above ~ 1250° C throughout the range of K_1 but below this temperature exhibits a two-stage behaviour, rising to $n \sim 40$ near to K_{IC} (~ 5 MPa m$^{1/2}$) with a reversal in temperature dependence. This is similar to the K_1–V characteristics for silicon nitride ceramics [2–4]. Ceramic C has a single value $n \sim 13$, is relatively insensitive to temperature with an increase in V for a constant K_1, typical of thermally activated processes. Hence, it is similar to the published data for recrystallized silicon carbide [21].

Fracture surfaces are predominantly intergranular for all crack velocities and temperatures in Fig. 7. However, the fracture-surface topography for ceramic B in the low-exponent part of the K_1–V relation is extremely rough, typical of a multiple branching of the primary crack during propagation. Both the lower temperature behaviour of ceramic B and that of ceramic C, throughout the range of temperature and velocity studied, is that of a relatively smooth fracture surface deviating by a few grain diameters from the mean plane. This difference in fracture surface topography is similar to previous observations of slow

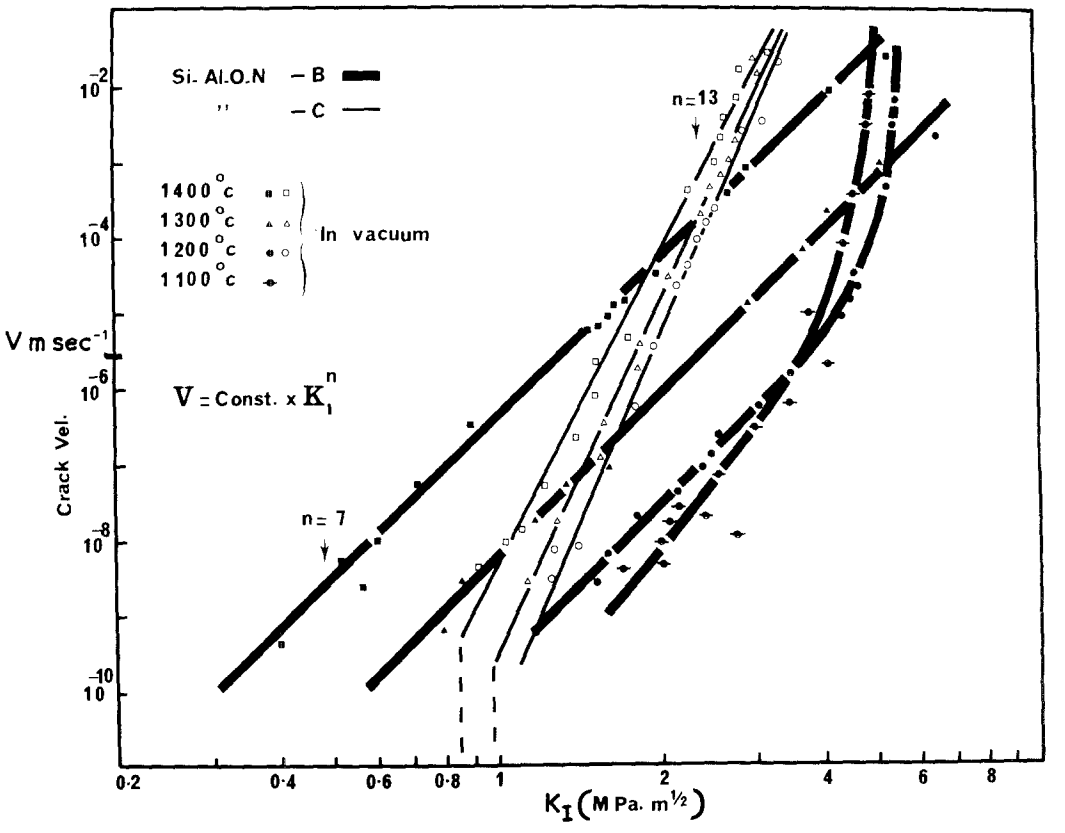

Figure 7 Sub-critical crack growth behaviour for the "cavitating" and "non-cavitating" ceramics B and C, demonstrated via the relation between crack velocity (V) and stress intensity factor (K_I). The dotted lines represent the K_I limit below which sub-critical crack growth is suppressed via diffusional creep in ceramic C.

and fast fracture surfaces during K_{IC} tests on single-edge notched beam specimens [5] and is visible in scanning electron micrographs (Fig. 8a and b).

The low exponent ($n < 10$), temperature sensitive, K_I–V relation and rough surface topography are characteristic of a mechanism for sub-critical crack growth via interlinkage of intergranular cavities, initiated by grain-boundary sliding. This is supported by the observation of creep-cavitation in ceramics A and B, and the appearance of multiple surface cracks and relatively low failure strains in bend creep specimens (Fig. 9a). This is in contrast with the non-cavitating ceramic C in which the low exponent K_I–V characteristic is absent and which suffers a comparatively large creep strain before fracture by the propagation of a single fast crack (Fig. 9b). The mechanism for sub-critical crack growth, which in the non-cavitating ceramic is restricted to a much narrower range of K_I, may be viewed as a thermally assisted breaking of atomic bonds between β' grains at the single intergranular crack front. The mechanism is not directly related to that for creep, hence the stress exponent and activation energies for the two mechanisms offer no comparison. A similar mechanism may be operative in the lower temperature/high velocity part of the K_I–V relation for ceramic B. The apparent reversal in temperature dependence in this region may result from a lowering in the real value of K_I (below that calculated from the macroscopic applied stress) with the onset of grain-boundary sliding at a rate sufficient to cause a "blunting" of the primary crack.

4.2. Failure prediction

The prediction of minimum times to failure for ceramic materials susceptible to sub-critical crack growth [2, 3] depends sensitively on a knowledge of K_I–V data in the region of low crack velocity. This may be obtained by direct microscopic measurement of crack position, under constant load conditions, and in this research has been extended to velocities $< 10^{-9}$ m sec^{-1} using

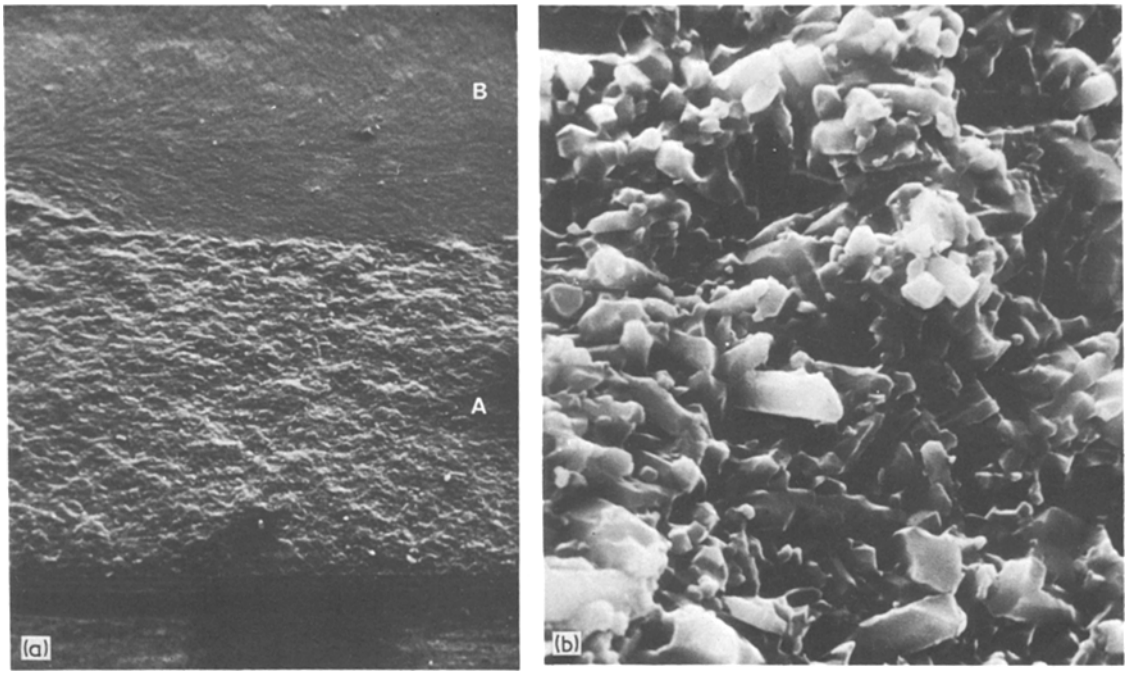

Figure 8 Scanning electron micrographs showing the differences in fracture surface topography between the region of sub-critical crack growth via a mechanism of cavitation (zone A, in (a) and at higher magnification in (b) and a region of fast fracture (zone B in (a)). A similar difference is apparent between ceramic C and ceramic B (in low exponent part of the K_1-V diagram) throughout the double-torsion fracture surface.

scanning electron microscopy. These measurements show that sub-critical crack growth is present in the cavitating ceramic (specimens A and B) for extremely small stress intensities ($K_1 \lesssim 0.05K_{IC}$ at 1400° C) and that extrapolation of the data using an empirical relation of the type $V = \text{constant}\ K_1^n$ is a reasonable procedure.

A similar experimental analysis for the non-cavitating ceramic (specimen C) produces the remarkable observation of zero crack velocity below a critical K_1 for a given temperature ($K_1 \lesssim 0.25K_{IC}$ at 1400° C, Fig. 7). A comparison of creep mechanisms for the two ceramics indicates that this suppression of sub-critical crack growth may result from crack-tip plasticity by diffusional creep which, at very low crack velocities, is effective in relaxing elastic stresses. Direct evidence for this mechanism is provided by a zone of anomalous contrast on the surface of notched double-torsion specimens which is present only after testing below the critical K_1 level (Fig. 10). This is believed to be a topographic contrast in the diffuse zone of stress-concentration at the notch tip, produced by grain rotation during diffusional creep. It is important to note that when a sharp crack has been initiated (above the critical K_1 before re-stressing below this level) a similar crack-stabilizing effect occurs but at a slightly lower critical K_1 and the plastic zone is not clearly resolved.

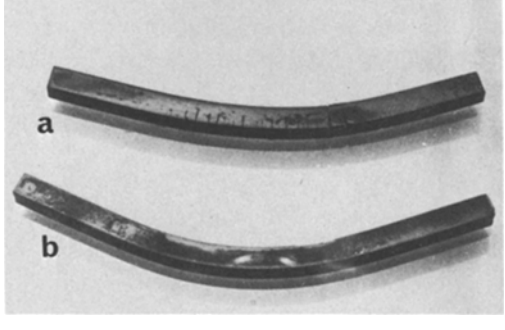

Figure 9 The macroscopic appearance of four-point bend creep specimens showing the effect of extensive cavitation on the appearance of multiple surface cracks and low failure strains for ceramic B (a). Ceramic C (b) rarely fails during the duration of a creep test and does so by the propagation of a single fast crack.

The suppression of sub-critical crack propagation in non-cavitating Si–Al–O–N ceramics is of great importance in relation to their application in the 1200 to 1400° C temperature interval. Time-

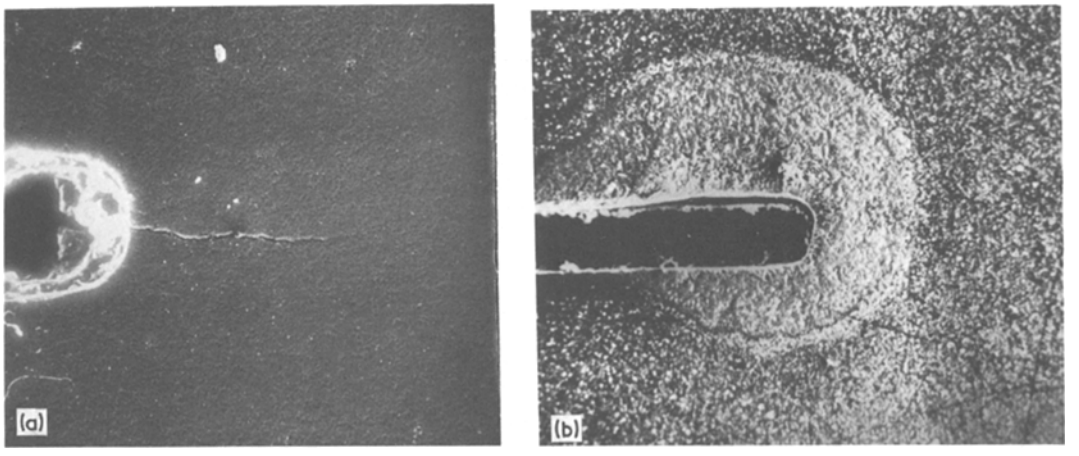

Figure 10 Scanning electron micrographs showing the propagation of a sharp sub-critical crack (a) and a suppression of crack growth in a zone of diffusional creep (b) at the initiating notch below a critical value of K_1.

dependent failure prediction procedures may be neglected for engineering components subjected to applied stresses below that resulting in K_1 values (for the dominant flaw geometry) smaller than the critical level at the maximum operating temperature.

The critical K_1 level, together with the exponent n in the K_1-V plot, may also be improved, in a similar manner to the creep behaviour, by heat-treatment in an oxidizing environment. The K_1-V data in Fig. 7 have been recorded under high-vacuum conditions and over short times compared

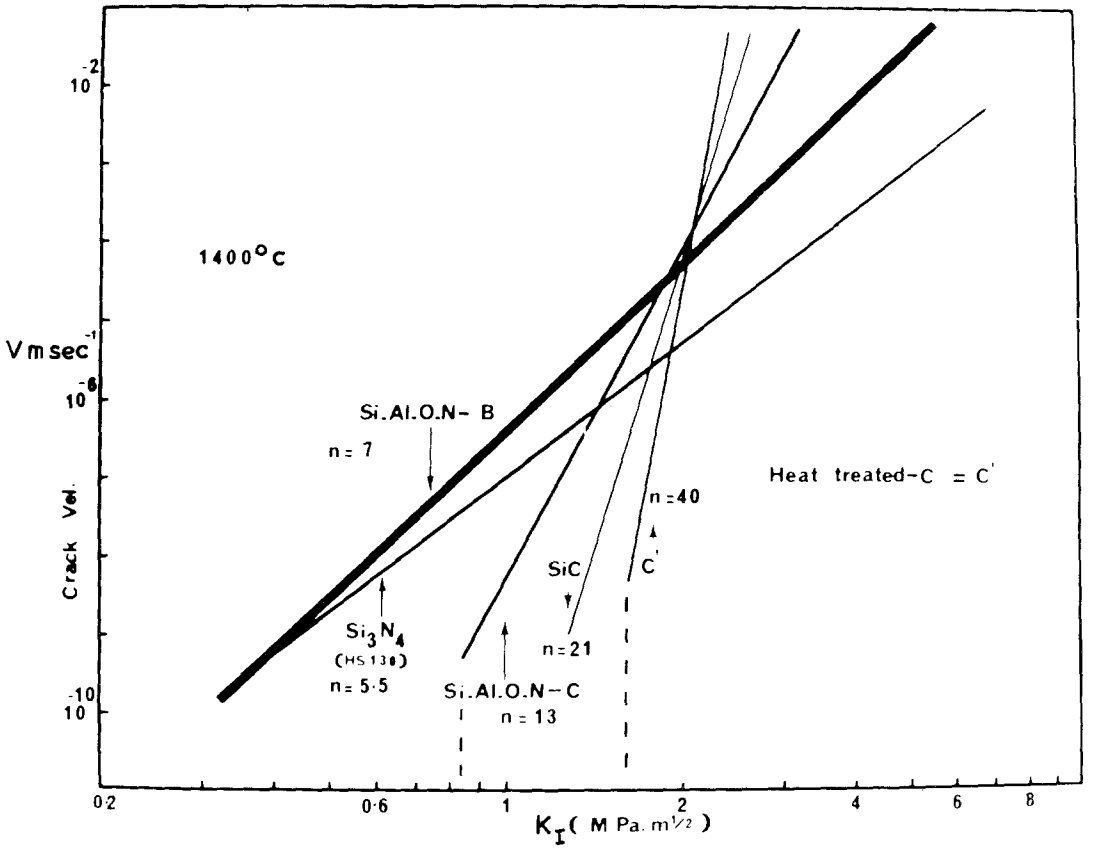

Figure 11 A comparison of K_1-V relationships at 1400° C for ceramics B and C with those for commercial Si_3N_4, SiC and ceramic C which has been heat-treated in an oxidizing environment before testing.

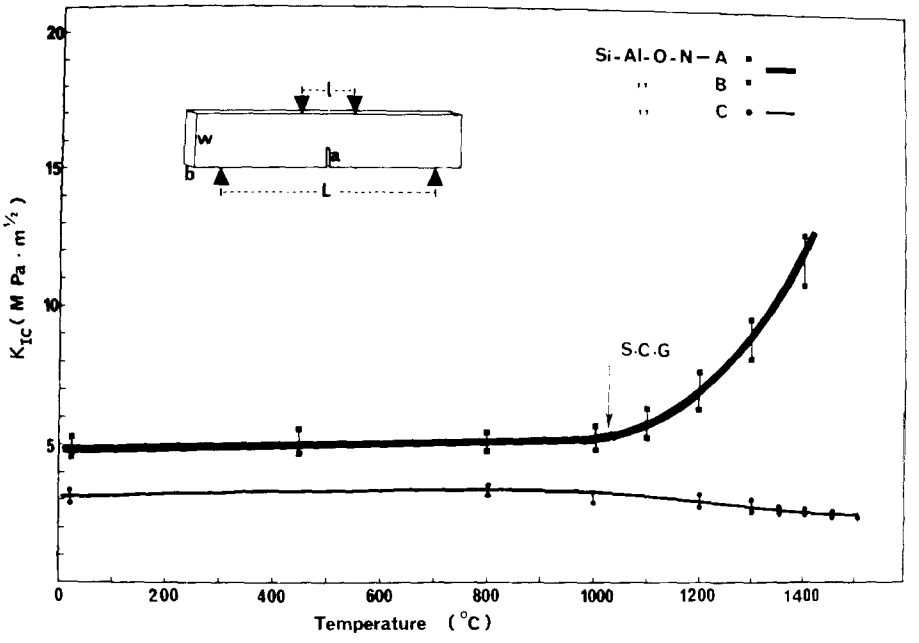

Figure 12 The variation in the critical stress-intensity factor (K_{IC}) for fast-fracture with temperature for the "cavitating" and "non-cavitating" ceramics.

with the creep tests, hence the time-dependent changes in grain-boundary structure are minimal. For specimens of ceramic C, heat-treated in air for ~900 h at 1400° C the values of n and the critical K_1 level are raised to 40 and $\sim 0.5 K_{IC}$, respectively, at 1400° C (Fig. 11). These values are changed little on increasing the test temperature to 1500° C and it is notable that the problem in maintaining a moderate vacuum at this temperature, due to specimen dissociation, is eliminated for the pre-oxidized specimens.

In Fig. 11 the 1400° C data for the "as hot-pressed" Si–Al–O–N ceramics are also replotted for comparison, together with published data for Si_3N_4 (HS130 grade) [2] and for SiC [21]. In making such comparisons one should note that the maximum K_1 for a particular ceramic is set by the value of K_{IC} (this is higher for ceramic B than for C) and that the K_1–V plot exhibits a small reduction in gradient with increased specimen thickness which is prominent only for the cavitating ceramic, increasing V by more than an order of magnitude in the 10^{-9} m sec^{-1} region [18].

4.3. Fracture toughness, K_{IC}

The critical stress intensity factor (K_{IC}) for fast fracture of Si_3N_4 ceramics generally lies between 3 and 6 MPa $m^{1/2}$. K_{IC} has previously been measured with varying temperature for the Mn-containing Si–Al–O–N (A) using the four-point bend (single edge-notched beam) test [5]. The measurements have been repeated for both ceramics (Fig. 12) and may be compared with the high-velocity limits observed on the K_1–V diagram (Fig. 7). There is reasonable agreement between these limits and the approximately temperature-independent values of 5 and 3 MPa $m^{1/2}$ for ceramics B and C respectively. However, the "cavitating" ceramic (B) exhibits the high-temperature increase in K_{IC} (Fig. 12), ascribed to the onset of intergranular plasticity, which is also characteristic of Si_3N_4 ceramics [22]. This is visible on K_{IC}–temperature diagrams only when the initial crack size is taken as the sawn notch depth together with the zone of sub-critical crack growth which occurs at stress intensities below K_{IC}, during loading [5, 22]. This high-temperature anomaly appears to be characteristic of (usually cavitating) ceramics which may undergo rapid grain-boundary sliding and is paralleled by the reversal in temperature dependence in the high K_1 region during the double-torsion test, discussed in Section 4.1.

A lower mean value of K_{IC} for ceramic C may result from its more equi-axed grain morphology, providing a less tortuous intergranular crack path. As discussed below, the cavitating ceramic is believed to retain a larger volume fraction of liquid silicate phase during the later stages of densification

and this favours an increase in the c/a ratio of grain dimension in the hexagonal prism morphology [23]. An alternative explanation is the crack-"blunting" effect of the relatively weak grain-boundaries normal to the direction of fast crack propagation in the cavitating ceramic. A difficulty with such explanations is the observation of a substantial fraction of transgranular fracture in both ceramics at low temperatures where the difference in K_{IC} is still apparent. However, a small transgranular fraction is retained at high temperatures only for the non-cavitating ceramic.

5. Grain boundary structure and high-temperature properties

5.1. The origin of cavitating behaviour

The principal contribution of the research described here has been to distinguish between high-temperature deformation mechanisms for Si–Al–O–N ceramics in terms of their susceptibility to intergranular creep cavitation. The microstructural feature believed to be responsible for cavity nucleation is the residual silicate phase located at β'-grain triple-junctions in ceramics prepared with a Mn additive. Within the limits of lattice-image resolution set by the β' prism plane spacing and the instrumental capability, grain boundaries in both types of ceramic contain no resolvable "phase". From the combined observations of lattice imaging and Auger electron spectroscopy it is concluded that segregated impurities (mainly the metallic additives Mg or Mn, the "accidental" impurity Ca, together with oxygen) are present at the boundary within a few atomic spacings of each crystal.

The triple-junction silicate in the Mn-containing ceramics, together with the high incidence of "special" grain boundaries containing prism-plane facets, suggests the presence of a larger quantity of silicate liquid in the final stages of sintering. It is believed that the essential difference between the two ceramics lies in the partitioning of Mg and Mn between the silicate phase and β' crystals. Hence, a smaller solubility of Mn in β' stabilizes the silicate phase in triple junctions after grain impingement, whereas the solid solution of Mg results in a greater probability for simultaneous solid solution of silicon and oxygen with further removal of residual silicate. An alternative explanation, that of an accidental difference in O/N balance from the β' requirement ($Si_{6-x}O_xAl_xN_{8-x}$), is not favoured in view of the reproducibility of the phenomenon with additive chemistry.

The inability to demonstrate a purely diffusional, non-cavitating, creep mechanism, or the control of sub-critical crack growth even in high purity Si_3N_4 ceramics containing Mg additives, demonstrates the importance of the Al substituted ceramic controlling the residual silicate phase [1]. Thus, the presence in β' of substituted Al may not only enable solid solution of charge-compensating oxygen, but may also permit the small Mg solubility in distorted interstitial sites as an alternative charge-compensating mechanism. X-ray microanalysis of β' grains indicates a Mg solubility of < 2 at.% which increases slightly with Al substitution level [24].

5.2. De-segregation

A reduction in the concentration of grain-boundary segregated elements has been accomplished by heat-treatment, preferably in an oxidizing environment. A minor part of the de-segregation may be attributed to a further solution within β' crystals as a result of non-equilibrium segregation at the end of the hot-pressing cycle. The major de-segregation mechanism is that of extraction of metallic ions into the SiO_2 oxidation layer, accompanied by a redistribution of other segregated elements (Si, O) between grain boundary and β' crystals. The increased density of covalent Si–N grain-boundary bonding enhances the cohesive energy of the interface and the activation-energy for diffusion of β' components in diffusional creep. This implication of a change in grain-boundary structure, rather than a change in grain-boundary silicate layer composition and hence viscosity, is supported by the remarkable observation of a retention of a large fraction of transgranular fracture even at 1500° C in heat-treated ceramics. Hence, in returning to the key question raised in the introductory section, it is extremely encouraging that this evidence favours the attainment of grain-boundary cohesion approaching that within the β' crystal.

It is interesting that the improvement in grain-boundary cohesion also produces a ceramic with a reduced susceptibility to dissocation, thereby enhancing its maximum temperature of application, and an increased low-temperature "hardness" which results in an increased difficulty of diamond machining.

Finally, the application of a grain-boundary de-

segregation process to a broader range of ceramics should be questioned. An intentional oxidation heat-treatment should also be effective in extracting metallic ions from the non-substituted Si_3N_4 ceramics, but the approach to the "pure" boundary structure may be limited by the restricted crystal solubility for oxygen. In this laboratory we have recently demonstrated the elimination of "cavitating" behaviour for the Mn-containing Si–Al–O–N following a long oxidizing heat-treatment [25]. However, the desegregation mechanism utilizes a long-range impurity diffusion and is likely to be inconvenient and expensive for bulk engineering components. It must be concluded that the most effective way to produce non-cavitating ceramic is to hot-press a carefully-balanced substituted β' Si–Al–O–N with a single (MgO) additive.

Acknowledgements

We wish to thank Dr R. J. Lumby and Mr B. North for preparation of the hot-pressed ceramics as part of our continuing collaborative research programme with the Lucas Group Research Centre, and Mr G. Smith for assistance with experimental work. B.S.B.K. is grateful for the award of a grant from the Commonwealth Scholarship Commission during the period of this research.

References

1. M. H. LEWIS, B. D. POWELL, P. DREW, R. J. LUMBY, B. NORTH and A. J. TAYLOR, *J. Mater. Sci.* **12** (1977) 61.
2. A. G. EVANS, in "Ceramics for High-Performance Applications", edited by Burke, Gorum and Katz (Brook-Hill, Mass., 1974) p. 373.
3. A. G. EVANS and S. M. WIEDERHORN, *J. Mater. Sci.* **9** (1974) 270.
4. N. J. TIGHE, *ibid* **13** (1978) 1455.
5. M. H. LEWIS and G. SMITH, in "Advances in Research on the Strength and Fracture of Materials", edited by D. M. R. Taplin (Pergamon, Oxford, 1977).
6. D. R. CLARKE and G. THOMAS, *J. Amer. Ceram. Soc.* **60** (1977) 491.
7. L. K. V. LOU, T. E. MITCHELL and A. H. HEUER, *ibid* **61** (1978) 392.
8. C. HERRING, *J. Appl. Phys.* **21** (1950) 437.
9. R. L. COBLE, *ibid* **34** (1963) 1679.
10. M. F. ASHBY and R. A. VERRALL, *Acta Met.* **21** (1973) 149.
11. A. H. HEUER, R. M. CANNON and N. J. TIGHE, in "Ultra fine-grain Ceramics", edited by J. J. Burke, N. L. Reed and V. Weiss (Syracuse University Press, New York, 1970).
12. S. U. DIN and P. S. NICHOLSON, *J. Mater. Sci.* **10** (1975) 1375.
13. R. KOSSOWSKY, D. G. MILLER and E. S. DIAZ, *ibid* **10** (1975) 983.
14. J. M. BIRCH and B. WILSHIRE, *ibid* **13** (1978) 2627.
15. N. J. OSBORNE, *Proc. Brit. Ceram. Soc.* **25** (1975) 263.
16. D. CUBICCIOTTI and K. H. LAU, *J. Amer. Ceram. Soc.* **61** (1978) 512.
17. M. H. LEWIS and P. BARNARD, *J. Mater. Sci.* **15** (1980) 443.
18. B. S. B. KARUNARATNE and M. H. LEWIS, *J. Amer. Ceram. Soc.* (to be submitted).
19. D. P. WILLIAMS and A. G. EVANS, *J. Test. Eval.* **1** (1973) 264.
20. A. G. EVANS, *J. Mater. Sci.* **7** (1972) 1137.
21. A. G. EVANS and F. F. LANGE, *ibid* **10** (1975) 1659.
22. J. L. HENSHALL, D. J. ROWCLIFFE and J. W. EDINGTON, *Special Ceramics* **6** (1975) 185.
23. M. H. LEWIS, A. R. BHATTI, R. J. LUMBY and B. NORTH, *J. Mater. Sci.* **15** (1980) 103.
24. *Idem, ibid.* 438.
25. B. S. B. KARUNARATNE and M. H. LEWIS (to be published).

Received 7 August and accepted 20 September 1979.